MULTIBEAM ANALOG BEAMFORMER DESIGN FOR MONOSTATIC ISAC UNDER SELF-INTERFERENCE

Jordi Borras[*]

Universitat Politècnica de Catalunya, Spain
jordi.borras@ieee.org

Roberto López-Valcarce[†]

atlanTTic, Universidade de Vigo, Spain
valcarce@gts.uvigo.es

ABSTRACT

Multibeam technology constitutes a key enabler for integrated sensing and communications (ISAC). Previous designs for millimeter-wave monostatic ISAC often overlook the self-interference (SI) induced on the co-located radar receiver and/or relax the hardware-imposed constant-modulus (CM) constraints. We address the multibeam optimization problem in monostatic ISAC with CM analog arrays, explicitly accounting for SI. First, we relax the CM constraints and provide a semi-analytic solution that illustrates the impact of SI on the communication-sensing tradeoff. The design is then adapted to CM analog beamformers, substantially reducing the performance loss incurred if CM constraints are naively imposed.

Index Terms— Integrated sensing and communications, multibeam, dual-functional radar-communications, analog beamforming.

1. INTRODUCTION

Integrated sensing and communications (ISAC) has been identified as a core technology for future wireless communications networks [1,2]. In ISAC systems, sensing and communication functions share the hardware platform, signaling and radio spectrum, which can provide mutual benefits and enable several applications envisioned in 6G, *e.g.,* autonomous driving, smart homes, and unmanned aerial vehicles (UAV) or vehicle-to-everything (V2X) networks [3,4].

Millimeter-wave (mmWave) spectrum is particularly well suited for ISAC, as large bandwidths allow resolving several multipath components, thus improving range resolution [5]. Moreover, small wavelengths imply compact large-aperture arrays that synthesize narrow beams, yielding high angular resolutions [6]. However, propagation at these frequencies suffers from severe path and penetration losses, requiring the use of directional beamforming [7].

Beamforming design for ISAC is challenging, especially with fully analog arrays using a single radio-frequency (RF) chain, given the different requirements of communication and sensing subsystems [8]. Multibeam beampattern design [9], also known as dual-functional beamforming, has been widely studied for balancing communication and sensing performances [4]. Most of the existing multibeam designs for hybrid or fully analog arrays are based on combining pre-designed *communication-optimal* and *sensing-optimal* solutions, via power control [10–15] or phase rotation and power control [16, 17]. Despite their simplicity and practicality, these designs only provide suboptimal solutions.

[*]Supported by MICIU/AEI/10.13039/501100011033 and by ERDF/EU under grant PID2022-136512OB-C21, and by grant 2021 SGR 01033.

[†]Supported by MICIU/AEI/10.13039/501100011033 and by ERDF/EU under grant PID2022-136512OB-C22.

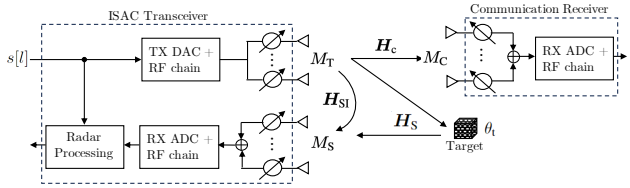

Fig. 1: Monostatic ISAC setting with phase-shifter based analog arrays. The ISAC transceiver serves a multi-antenna communication receiver while simultaneously monitoring a target located at direction θ_{t}.

Global optimal solutions for fully digital beamformers are discussed in, *e.g.,* [14, 18–21]. However, these architectures are impractical at mmWave, since a dedicated per-antenna RF chain and a digital-to-analog converter/analog-to-digital converter (DAC/ADC) entail prohibitive power consumption. For fully analog arrays, [17] provides an optimal multibeam design, but incorporating per-antenna gain control to circumvent the intractable constant-modulus (CM) constraints inherent to the use of phase shifters. Moreover, [17] also overlooks the self-interference (SI) induced by the transmit array on the sensing array in monostatic settings. Some works dealing with SI typically use not only transmit beamforming but also RF cancellation at the radar receiver [11, 22]. While this is effective to prevent ADC saturation, it adds complexity and cost, and RF components preceding the SI analog canceler remain unprotected.

We present a novel analog multibeam design that explicitly accounts for SI and CM design constraints. First, we provide a semi-analytic relaxed optimal solution exhibiting maximum beamforming gain for communications while guaranteeing the required beamforming gain for sensing and limiting the *transmitted* SI. The proposed adaptation of this design scheme to incorporate CM constraints improves previous analog designs in balancing the three-fold tradeoff between communication, sensing, and SI cancellation.

2. PROBLEM SETTING

Consider the mmWave scenario of Fig. 1, in which an ISAC transceiver equipped with separate transmit-sensing analog arrays simultaneously serves a multi-antenna communication node with M_{C} antennas and tracks a target located at a certain known direction. The ISAC transceiver has M_{T} transmit and M_{S} sensing antennas.

We assume CM phased arrays, *i.e.*, each antenna is connected to a phase shifter with no individual gain control. The transmit, sensing, and receive beamforming vectors are respectively denoted $\boldsymbol{f} \in \mathbb{C}^{M_{\mathrm{T}}}$, $\boldsymbol{w}_{\mathrm{s}} \in \mathbb{C}^{M_{\mathrm{S}}}$, and $\boldsymbol{w}_{\mathrm{c}} \in \mathbb{C}^{M_{\mathrm{C}}}$. The analog implementation shown in Fig. 1 imposes constraints on their entries, so that $\boldsymbol{f} \in \mathbb{V}^{M_{\mathrm{T}}}$, $\boldsymbol{w}_{\mathrm{s}} \in \mathbb{V}^{M_{\mathrm{S}}}$, and $\boldsymbol{w}_{\mathrm{c}} \in \mathbb{V}^{M_{\mathrm{C}}}$, with

$$\mathbb{V}^m \triangleq \{\boldsymbol{x} \in \mathbb{C}^m \ : \ |x_i| = 1, \ 1 \le i \le m\}\,. \tag{1}$$

It is assumed that the communication channel $\boldsymbol{H}_{\rm c} \in \mathbb{C}^{M_{\rm C}\times M_{\rm T}}$, the SI channel $\boldsymbol{H}_{\rm SI} \in \mathbb{C}^{M_{\rm S}\times M_{\rm T}}$, and the target response matrix $\boldsymbol{H}_{\rm S} \in \mathbb{C}^{M_{\rm S}\times M_{\rm T}}$ are frequency-flat, as in [17]. This assumption implies narrowband transmission and that the beam squint effect on the steering vectors is negligible. We also assume that $\boldsymbol{H}_{\rm c}$ and $\boldsymbol{H}_{\rm SI}$ have been estimated *a priori* using pilot-assisted mmWave channel acquisition techniques (see, e.g., [1, Sec. III-B]).

The ISAC transceiver sends a data stream $\{s[l]\}$, with l indexing the channel use, of complex zero-mean, unit-variance symbols, so that the transmitted signal reads as $\boldsymbol{x}[l] = \boldsymbol{f}s[l] \in \mathbb{C}^{M_{\rm T}}$. After receive processing, the received baseband communication signal is

$$y[l] = \boldsymbol{w}_{\rm c}^H \boldsymbol{H}_{\rm c}\boldsymbol{f}s[l] + \boldsymbol{w}_{\rm c}^H \boldsymbol{n}_{\rm c}[l], \tag{2}$$

where $\boldsymbol{n}_{\rm c}[l] \sim \mathcal{N}_{\mathbb{C}}(\boldsymbol{0}, \sigma_{\rm c}^2 \boldsymbol{I}_{M_{\rm C}})$ is circularly-symmetric Gaussian noise. Note that, for given transmit beamformer $\boldsymbol{f}$, the optimal receive beamformer is an equal-gain combiner with

$$[\boldsymbol{w}_{\rm c}]_i = e^{\imath \measuredangle [\boldsymbol{H}_{\rm c}\boldsymbol{f}]_i},\ i \in \{1, \ldots, M_{\rm C}\}. \tag{3}$$

The co-located radar suffers from SI when the isolation between TX and sensing arrays is weak and the length of $\{s[l]\}$ is larger than the target's echo round-trip time. Thus, the radar observation reads as

$$r[l] = \boldsymbol{w}_{\rm s}^H \boldsymbol{H}_{\rm S}\boldsymbol{f}s[l] + \underbrace{\boldsymbol{w}_{\rm s}^H \boldsymbol{H}_{\rm SI}\boldsymbol{f}s[l]}_{\text{Post-combining SI}} + \boldsymbol{w}_{\rm s}^H \boldsymbol{n}_{\rm s}[l], \tag{4}$$

with $\boldsymbol{n}_{\rm s}[l] \sim \mathcal{N}_{\mathbb{C}}(\boldsymbol{0}, \sigma_{\rm s}^2 \boldsymbol{I}_{M_{\rm S}})$ the sensing noise. SI not only degrades radar performance, but it can also saturate the RF components of the sensing array. Typically, transmit and sensing beamformers $\boldsymbol{f}$, $\boldsymbol{w}_{\rm s}$ are jointly designed to maximally suppress the post-combining SI (see, *e.g.*, [11, 15]). Despite their effectiveness in avoiding ADC saturation and improving sensing performance, these approaches need not avoid saturation of the RF circuitry preceding the analog combiner [23]. In this regard, the *pre-combining* SI power

$$P_{\rm SI} \triangleq \mathbb{E}\{\|\boldsymbol{H}_{\rm SI}\boldsymbol{f}s[l]\|^2\} = \boldsymbol{f}^H \boldsymbol{H}_{\rm SI}^H \boldsymbol{H}_{\rm SI}\boldsymbol{f} \tag{5}$$

should be kept below a threshold so that all RF components preceding $\boldsymbol{w}_{\rm s}$ operate within the linear region. With this in mind, our goal is to design the CM analog transmit beamformer $\boldsymbol{f}$ to maximize the communication beamforming gain, given by

$$G_{\text{tx,comm}} \triangleq \boldsymbol{f}^H \boldsymbol{H}_{\rm c}^H \boldsymbol{H}_{\rm c}\boldsymbol{f}, \tag{6}$$

while keeping the pre-combining SI power in (5) below a threshold η^2 and the beamforming gain for sensing, given by

$$G_{\text{tx,sen}}(\theta_{\rm t}) \triangleq \left|\boldsymbol{f}^H \boldsymbol{a}_{\rm T}(\theta_{\rm t})\right|^2, \tag{7}$$

above a preset threshold τ^2. In (7), $\boldsymbol{a}_{\rm T}(\theta)$ denotes the transmit array steering vector at direction θ, satisfying $\|\boldsymbol{a}_{\rm T}(\theta)\|^2 = M_{\rm T}$. Note that, once $\boldsymbol{f}$ is available, $\boldsymbol{w}_{\rm c}$ is given by (3), whereas $\boldsymbol{w}_{\rm s}$ can be designed following a maximal radar signal-to-interference-plus-noise ratio (SINR) rule as in [24]. Next we focus on the design of the transmit beamformer $\boldsymbol{f}$.

3. SI-AWARE CM ANALOG MULTIBEAM DESIGN

Next we present a CM analog beamformer design scheme for monostatic ISAC accounting for the impact of SI. Initially, in Sec. 3.1 we relax the CM constraints and address the problem under a total power constraint. This provides an insightful semi-analytic solution that will be appropriately modified in Sec. 3.2 to handle the intractable CM constraints.

3.1. Design under a total power constraint

Individual gain control can be achieved by including a variable-gain amplifier (VGA) per antenna. The CM constraint $\boldsymbol{f} \in \mathbb{V}^{M_{\rm T}}$ is thus replaced by a norm constraint on $\boldsymbol{f}$, and the design problem reads as

$$\max_{\boldsymbol{f}\in\mathbb{C}^{M_{\rm T}}} \quad G_{\text{tx,comm}} \tag{8a}$$

$$\text{s.t.} \quad \text{(a) } G_{\text{tx,sen}}(\theta_{\rm t}) \geq \tau^2,\ \text{(b) } P_{\rm SI} \leq \eta^2,\ \text{(c) } \|\boldsymbol{f}\|^2 = M_{\rm T}. \tag{8b}$$

Note that (8) is feasible iff $\eta^2 \geq M_{\rm T}\lambda_{\min}\left(\boldsymbol{H}_{\rm SI}^H \boldsymbol{H}_{\rm SI}\right)$, $\tau^2 \leq M_{\rm T}\|\boldsymbol{a}_{\rm T}(\theta_{\rm t})\|^2$ and $G_{\text{tx,sen}}^{\star}(\theta_{\rm t}) \geq \tau^2$, where

$$G_{\text{tx,sen}}^{\star}(\theta_{\rm t}) \triangleq \max_{\boldsymbol{f}\in\mathbb{C}^{M_{\rm T}}} G_{\text{tx,sen}}(\theta_{\rm t}) \quad \text{s.t.} \quad P_{\rm SI} \leq \eta^2,\ \|\boldsymbol{f}\|^2 = M_{\rm T}. \tag{9}$$

Note that (8) is a quadratically constrained quadratic program (QCQP) with three constraints, so it can be solved, if feasible, via semidefinite relaxation (SDR) [25, 26]. However, to gain some insight into the CM design to be discussed in Sec. 3.2, we adopt a different approach to obtain a semi-analytic solution. Define the $M_{\rm T} \times M_{\rm T}$ positive semidefinite matrices $\boldsymbol{A} \triangleq \boldsymbol{H}_{\rm c}^H \boldsymbol{H}_{\rm c}$, $\boldsymbol{B} \triangleq \boldsymbol{a}_{\rm T}(\theta_{\rm t})\boldsymbol{a}_{\rm T}^H(\theta_{\rm t})$, $\boldsymbol{C} \triangleq \boldsymbol{H}_{\rm SI}^H \boldsymbol{H}_{\rm SI}$, and let $\boldsymbol{H}(\mu,\gamma) \triangleq \boldsymbol{A} + \mu\boldsymbol{B} - \gamma\boldsymbol{C}$, where $\mu \geq 0$, $\gamma \geq 0$ are the Lagrange multipliers for constraints (a) and (b) in (8b). Then, the Lagrangian for problem (8) reads as

$$\mathcal{L}(\boldsymbol{f},\mu,\gamma,\lambda) = \boldsymbol{f}^H\left(-\boldsymbol{H}(\mu,\gamma) + \lambda\boldsymbol{I}_{M_{\rm T}}\right)\boldsymbol{f} + \mu\tau^2 - \gamma\eta^2 - \lambda M_{\rm T}, \tag{10}$$

where λ is the Lagrange multiplier associated with constraint (c) in (8b). Appendix A shows that the optimal solution for (8) is given by

$$\boldsymbol{f}_{\star} = \sqrt{M_{\rm T}}\mathcal{D}\left[\boldsymbol{H}(\mu_{\star},\gamma_{\star})\right], \tag{11}$$

where $\mathcal{D}[\boldsymbol{X}]$ returns the dominant unit-norm eigenvector of $\boldsymbol{X}$. Since the optimal values $\mu_{\star}$, $\gamma_{\star}$ do not admit a closed-form solution, we undertake the following procedure to attempt to solve (8):

1. First, check whether the solution obtained by relaxing constraints (a) and (b) in (8b) is feasible, in which case $\boldsymbol{f}_{\star} = \sqrt{M_{\rm T}}\mathcal{D}[\boldsymbol{A}]$ solves (8). Otherwise, proceed to Step 2.
2. Relaxing either constraint (a) or (b) in (8b), solve:

$$\boldsymbol{f}_{(a)} = \arg\max_{\boldsymbol{f}\in\mathbb{C}^{M_{\rm T}}} G_{\text{tx,comm}} \quad \text{s.t.} \quad G_{\text{tx,sen}} = \tau^2,\ \|\boldsymbol{f}\|^2 = M_{\rm T}, \tag{12}$$

$$\boldsymbol{f}_{(b)} = \arg\max_{\boldsymbol{f}\in\mathbb{C}^{M_{\rm T}}} G_{\text{tx,comm}} \quad \text{s.t.} \quad P_{\rm SI} = \eta^2,\ \|\boldsymbol{f}\|^2 = M_{\rm T}. \tag{13}$$

Let $\alpha \triangleq \boldsymbol{f}_{(a)}^H \boldsymbol{C}\boldsymbol{f}_{(a)}$ and $\beta \triangleq \boldsymbol{f}_{(b)}^H \boldsymbol{B}\boldsymbol{f}_{(b)}$. Then, the solution $\boldsymbol{f}_{\star}$ to (8) is given by

$$\boldsymbol{f}_{\star} = \begin{cases} \boldsymbol{f}_{(a)} & \text{if } \alpha \leq \eta^2 \text{ and } \beta \leq \tau^2, \\ \boldsymbol{f}_{(b)} & \text{if } \alpha \geq \eta^2 \text{ and } \beta \geq \tau^2, \\ \underset{\{\boldsymbol{f}_{(a)},\boldsymbol{f}_{(b)}\}}{\arg\max}\ G_{\text{tx,comm}} & \text{if } \alpha \leq \eta^2 \text{ and } \beta \geq \tau^2. \end{cases} \tag{14}$$

If $\alpha \geq \eta^2$ and $\beta \leq \tau^2$, proceed to Step 3.

3. When both constraints (a) and (b) in (8) are active, *i.e.*, $\mu > 0$ and $\gamma > 0$, the optimal $\mu_{\star}$ and $\gamma_{\star}$ are such that constraints (a) and (b) are simultaneously satisfied with equality, *i.e.*, $\boldsymbol{f}_{\star}^H \boldsymbol{B}\boldsymbol{f}_{\star}^H = \tau^2$ and $\boldsymbol{f}_{\star}^H \boldsymbol{C}\boldsymbol{f}_{\star}^H = \eta^2$.

Regarding Step 2, the structure of $\boldsymbol{f}_{(a)}$ and $\boldsymbol{f}_{(b)}$ can be inferred from Appendix A (by setting $\gamma = 0$ or $\mu = 0$), and is given by

$$\boldsymbol{f}_{(a)} = \sqrt{M_{\rm T}}\mathcal{D}\left[\boldsymbol{A} + \mu_{\star}\boldsymbol{B}\right], \quad \boldsymbol{f}_{(b)} = \sqrt{M_{\rm T}}\mathcal{D}\left[\boldsymbol{A} - \gamma_{\star}\boldsymbol{C}\right], \tag{15}$$

where $\mu_\star$ and $\gamma_\star$ are such that $\boldsymbol{f}_{(a)}^H \boldsymbol{B} \boldsymbol{f}_{(a)} = \tau^2$ and $\boldsymbol{f}_{(b)}^H \boldsymbol{C} \boldsymbol{f}_{(b)} = \eta^2$, respectively, and can be found via line search.

As for Step 3, one must find the values of $\mu, \gamma \in [0, \infty)$ at which the principal eigenvector of $\boldsymbol{H}(\mu, \gamma)$ simultaneously satisfies constraints (a) and (b) in (8b) with equality. To reduce the search space for μ and γ, we will consider the matrix

$$\frac{1}{1+\mu+\gamma} \boldsymbol{H}(\mu, \gamma) = (1 - \alpha_1 - \alpha_2)\boldsymbol{A} + \alpha_1 \boldsymbol{B} - \alpha_2 \boldsymbol{C}, \quad (16)$$

with $\alpha_1 = \frac{\mu}{1+\mu+\gamma} \in [0, 1]$, $\alpha_2 = \frac{\gamma}{1+\mu+\gamma} \in [0, 1 - \alpha_1]$. Note that (16) has the same eigenvectors as $\boldsymbol{H}(\mu, \gamma)$. Letting $\boldsymbol{\alpha} \triangleq [\alpha_1, \alpha_2]^T$ and $\boldsymbol{u} \triangleq \sqrt{M_\mathrm{T}} \mathcal{D}[(1 - \boldsymbol{\alpha}^T \boldsymbol{1})\boldsymbol{A} + \alpha_1 \boldsymbol{B} - \alpha_2 \boldsymbol{C}]$, the problem amounts to finding the roots of $\boldsymbol{q} : \mathbb{R}^2 \to \mathbb{R}^2$ defined by

$$\boldsymbol{q}(\boldsymbol{\alpha}) \triangleq \begin{bmatrix} q_1(\boldsymbol{\alpha}) \\ q_2(\boldsymbol{\alpha}) \end{bmatrix} = \begin{bmatrix} \boldsymbol{u}^H \boldsymbol{B} \boldsymbol{u} - \tau^2 \\ \boldsymbol{u}^H \boldsymbol{C} \boldsymbol{u} - \eta^2 \end{bmatrix}. \quad (17)$$

Since both $q_1(\boldsymbol{\alpha})$ and $q_2(\boldsymbol{\alpha})$ are nonlinear, one has to resort to root-finding schemes. We propose using the Newton-Raphson method [27, Ch. 7], which iteratively updates the root of (17) as

$$\boldsymbol{\alpha}_{n+1} = \boldsymbol{\alpha}_n - \boldsymbol{J}_{\boldsymbol{q}}^{-1}(\boldsymbol{\alpha}_n) \boldsymbol{q}(\boldsymbol{\alpha}_n), \quad (18)$$

where $\boldsymbol{J}_{\boldsymbol{q}}(\boldsymbol{\alpha})$ is the Jacobian matrix of $\boldsymbol{q}(\boldsymbol{\alpha})$ (whose derivation is given in Appendix B), with $[\boldsymbol{J}_{\boldsymbol{q}}(\boldsymbol{\alpha})]_{ij} = \frac{\partial}{\partial \alpha_j} q_i(\boldsymbol{\alpha})$. This approach has to be run until convergence, *i.e.*, until there is a root such that constraints (a) and (b) in (8b) are met within a sufficiently small tolerance ϵ. The Newton-Raphson method converges fast, but it needs a sufficiently accurate initial estimate of the root. We have observed that 2D bisection search with moderate tolerance (*e.g.,* 10^{-2}) suffices to efficiently obtain a good initialization.

3.2. Design under CM constraints

Restoring the original CM constraints, the problem now reads as

$$\max_{\boldsymbol{f}} \quad G_{\text{tx,comm}} \quad (19a)$$

$$\text{s.t.} \quad \text{(a) } G_{\text{tx,sen}}(\theta_\mathrm{t}) \geq \tau^2, \quad \text{(b) } P_{\text{SI}} \leq \eta^2, \quad \text{(c) } \boldsymbol{f} \in \mathbb{V}^{M_\mathrm{T}}. \quad (19b)$$

Some options to enforce the original CM constraints are as follows. The first one is straightforward and consists in projecting the norm-constrained solution from Sec. 3.1 onto the set of CM vectors $\mathbb{V}^{M_\mathrm{T}}$, which is done by dividing each entry by its modulus. However, this may yield a CM beamformer not meeting constraints (a) or (b) in (8b). In the second approach the CM constraints are squared up, replacing $|f_i| = 1$ by $|f_i|^2 = 1$, and then the resulting QCQP with $M_\mathrm{T} + 2$ constraints is addressed via SDR. However, this approach is not tight in general.

As a third alternative, we propose modifying the three-step procedure described in Sec. 3.1 to enforce the CM constraint (c) in (19b) at each iteration of the bisection search in Step 2 and of the Newton-Raphson method in Step 3. Due to space limitations, we just sketch this procedure as Algorithm 1, where $\mathcal{P}_{\mathbb{V}^n}\{\boldsymbol{x}\}$ represents the projection of $\boldsymbol{x} \in \mathbb{C}^n$ onto $\mathbb{V}^n$.

4. NUMERICAL EXAMPLE

The proposed algorithm is tested in the scenario shown in Fig. 1, adopting at the ISAC transceiver the array geometry described in [28, Fig. 2] with $\alpha = \beta = \frac{\pi}{2}$ and $\delta = 2\lambda$ (λ is the carrier wavelength). Both communication and SI channels are modeled as in [28]. For the communication channel, we adopt the Saleh-Valenzuela narrowband clustered model with N_{cluster} clusters and N_{ray} rays per cluster:

$$\boldsymbol{H}_\mathrm{c} = \sum\nolimits_{i=1}^{N_{\text{cluster}}} \sum\nolimits_{j=1}^{N_{\text{ray}}} g_{ij} \boldsymbol{a}_\mathrm{R}(\phi_{ij}) \boldsymbol{a}_\mathrm{T}^H(\theta_{ij}), \quad (20)$$

where g_{ij}, θ_{ij}, and ϕ_{ij} denote complex path gains, angles of departure (AoD), and angles of arrival (AoA), respectively; and $\boldsymbol{a}_\mathrm{T}(\theta)$, $\boldsymbol{a}_\mathrm{R}(\phi)$ denote the TX and RX array steering vectors, with $\|\boldsymbol{a}_\mathrm{T}(\theta)\|^2 = M_\mathrm{T}$, $\|\boldsymbol{a}_\mathrm{R}(\phi)\|^2 = M_\mathrm{C}$ $\forall \theta, \phi$. We assume that the SI channel has a Line-of-Sight (LOS) component due to near-field coupling, modeled as $[\boldsymbol{H}_{\text{SI}}^{(\text{LOS})}]_{pq} = \frac{1}{r_{pq}} \exp\{\frac{-\imath 2\pi r_{pq}}{\lambda}\}$, with r_{pq} the distance between the q-th TX and p-th RX array elements. The Non-LOS (NLOS) component $\boldsymbol{H}_{\text{SI}}^{(\text{NLOS})}$ is due to reflections by nearby scatters and is modeled analogously to (20). With this, after normalizing so that $\|\boldsymbol{H}_{\text{SI}}^{(\text{LOS})}\|_\mathrm{F}^2 = \|\boldsymbol{H}_{\text{SI}}^{(\text{NLOS})}\|_\mathrm{F}^2 = M_\mathrm{T} M_\mathrm{S}$, the SI channel is obtained as $\boldsymbol{H}_{\text{SI}} = \sqrt{\frac{\kappa}{1+\kappa}} \boldsymbol{H}_{\text{SI}}^{(\text{LOS})} + \sqrt{\frac{1}{1+\kappa}} \boldsymbol{H}_{\text{SI}}^{(\text{NLOS})}$, where κ is the Rice factor. In the simulation, we considered $M_\mathrm{T} = 32$, $M_\mathrm{S} = 8$, and $M_\mathrm{C} = 16$, $N_{\text{cluster}} = 7$, $N_{\text{ray}} = 5$, and $\kappa = 10$ dB. AoDs, AoAs, and the target direction are assumed Gaussian distributed, with mean angle uniformly distributed over $[0, 360^\circ]$ and standard deviation 8°. Complex path gains are also Gaussian distributed with mean 1.2589 (corresponding to 1 dB) and variance 1.122 (corresponding to 0.5 dB). Channel matrices are normalized so that $\|\boldsymbol{H}_\mathrm{c}\|_\mathrm{F}^2 = M_\mathrm{T} M_\mathrm{C}$ and $\|\boldsymbol{H}_{\text{SI}}\|_\mathrm{F}^2 = M_\mathrm{T} M_\mathrm{S}$.

With respect to the optimization problem (19), we let $\tau^2 \in [0, M_\mathrm{T}^2]$. Regarding to η^2, it must limit the maximum SI leaked into the sensing array, which is given by $M_\mathrm{T} \lambda_{\max}(\boldsymbol{H}_{\text{SI}}^H \boldsymbol{H}_{\text{SI}}) = M_\mathrm{T} s_{\max}(\boldsymbol{H}_{\text{SI}})$ ($s_{\max}(\boldsymbol{X})$ returns the maximum singular value of matrix $\boldsymbol{X}$). Since $M_\mathrm{T} s_{\max}(\boldsymbol{H}_{\text{SI}}) \leq M_\mathrm{T} \|\boldsymbol{H}_{\text{SI}}\|_\mathrm{F}^2 = M_\mathrm{T}^2 M_\mathrm{S}$, we

Algorithm 1: Proposed CM Analog Beamforming Design

Input: $\boldsymbol{A}, \boldsymbol{B}, \boldsymbol{C}, \tau^2, \eta^2$ $\epsilon, \omega_{\min} = 0, \omega_{\max} = 1, \boldsymbol{\alpha}_0$
Output: $\boldsymbol{f}_\star$

Set $\boldsymbol{f} \leftarrow \mathcal{P}_{\mathbb{V}^{M_\mathrm{T}}}\{\mathcal{D}[\boldsymbol{A}]\}$;
if $\boldsymbol{f}^H \boldsymbol{B} \boldsymbol{f} < \tau^2$ *or* $\boldsymbol{f}^H \boldsymbol{C} \boldsymbol{f} > \eta^2$ **then**
  $\boldsymbol{f}_{(a)} \leftarrow \text{CMBisection}(\boldsymbol{A}, \boldsymbol{B}, \tau^2, \epsilon, \omega_{\min}, \omega_{\max})$;
  $\boldsymbol{f}_{(b)} \leftarrow \text{CMBisection}(\boldsymbol{A}, \boldsymbol{C}, \eta^2, \epsilon, \omega_{\min}, \omega_{\max})$;
  if $\boldsymbol{f}_{(a)}^H \boldsymbol{C} \boldsymbol{f}_{(a)} > \eta^2$ *and* $\boldsymbol{f}_{(b)}^H \boldsymbol{B} \boldsymbol{f}_{(b)} < \tau^2$ **then**
    $\boldsymbol{f} \leftarrow \text{CMNewton}(\boldsymbol{A}, \boldsymbol{B}, \boldsymbol{C}, \tau^2, \eta^2, \epsilon, \boldsymbol{\alpha}_0)$;
  else
    Find $\boldsymbol{f}$ via (14);
  end
end
$\boldsymbol{f}_\star \leftarrow \boldsymbol{f}$;

Function $\text{CMBisection}(\boldsymbol{X}, \boldsymbol{Y}, \beta, \epsilon, \omega_{\min}, \omega_{\max})$
  repeat
    $\omega \leftarrow (\omega_{\min} + \omega_{\max})/2$;
    $\boldsymbol{g} \leftarrow \mathcal{P}_{\mathbb{V}^{M_\mathrm{T}}}\{\mathcal{D}[(1-\omega)\boldsymbol{X} + \omega \boldsymbol{Y}]\}$;
    if $\boldsymbol{g}^H \boldsymbol{Y} \boldsymbol{g} > \beta$, **then** $\omega_{\max} \leftarrow \omega$;
    else, $\omega_{\min} \leftarrow \omega$, **end**;
  until $|\boldsymbol{g}^H \boldsymbol{Y} \boldsymbol{g} - \beta| \leq \epsilon$;
  return $\boldsymbol{g}$
end

Function $\text{CMNewton}(\boldsymbol{X}, \boldsymbol{Y}, \boldsymbol{Z}, \beta_1, \beta_2, \epsilon, \boldsymbol{\alpha}_0)$
  $\boldsymbol{u} \leftarrow \mathcal{P}_{\mathbb{V}^{M_\mathrm{T}}}\{\mathcal{D}[(1 - \boldsymbol{\alpha}_0^T \boldsymbol{1})\boldsymbol{X} + \boldsymbol{\alpha}_0[1]\boldsymbol{Y} - \boldsymbol{\alpha}_0[2]\boldsymbol{Z}]\}$;
  repeat
    Update $\boldsymbol{\alpha}$ via (17)-(18);
    $\boldsymbol{u} \leftarrow \mathcal{P}_{\mathbb{V}^{M_\mathrm{T}}}\{\mathcal{D}[(1 - \boldsymbol{\alpha}^T \boldsymbol{1})\boldsymbol{X} + \boldsymbol{\alpha}[1]\boldsymbol{Y} - \boldsymbol{\alpha}[2]\boldsymbol{Z}]\}$;
  until $|\boldsymbol{u}^H \boldsymbol{Y} \boldsymbol{u} - \beta_1| \leq \epsilon$ *and* $|\boldsymbol{u}^H \boldsymbol{Z} \boldsymbol{u} - \beta_2| \leq \epsilon$;
  return $\boldsymbol{u}$
end

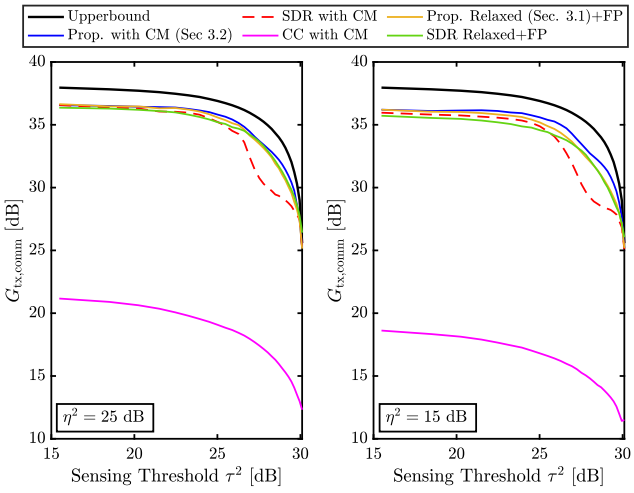

Fig. 2: Beamforming gain for communications (6) vs. the preset sensing threshold τ^2 for $\eta^2 = 25$ dB (left) and $\eta^2 = 15$ dB (right) obtained with the proposed method and the considered benchmarks.

set $\eta^2 = \zeta M_{\text{T}}^2 M_{\text{S}}$, with $\zeta \in \{\frac{1}{250}, \frac{1}{25}\}$, which corresponds to $\eta^2 \in \{15, 25\}$ dB with the simulation parameters adopted. As benchmarks, we considered: (*i*) *SDR with CM*: solving (19) via SDR and obtaining a rank-one solution through eigendecomposition (EVD); (*ii*) *CC with CM*: a convex combination (CC) of the communication optimal solution (under maximum SI and CM constraints) $\boldsymbol{f}_{\text{com}}$ and the sensing optimal solution (under maximum SI and CM constraints) $\boldsymbol{f}_{\text{sen}}$, *i.e.*, $\boldsymbol{f} = \rho \boldsymbol{f}_{\text{com}} + (1-\rho)\boldsymbol{f}_{\text{sen}}$, with ρ found via bisection search to satisfy the sensing constraint and a final projection (FP) onto $\mathbb{V}^{M_{\text{T}}}$; (*iii*) *Prop. Relaxed+FP*: the projection onto $\mathbb{V}^{M_{\text{T}}}$ of the proposed relaxed design of Sec. 3.1; and (*iv*) *SDR Relaxed+FP*: solving (8) via SDR, extracting a rank-one solution via EVD, and projecting the result onto $\mathbb{V}^{M_{\text{T}}}$. For reference, we show the communication-sensing upper bound, *i.e.,* solving (8) neglecting the SI constraint.

Fig. 2 illustrates the achieved communication beamforming gain versus the sensing threshold τ^2 and for two SI thresholds, averaged over 500 Monte Carlo trials. It is seen that the proposed algorithm in Sec. 3.2 achieves a communication-sensing performance close to the upper bound for both values of η^2. Except for benchmark (*ii*), the other ones track the proposed method closely, especially at low-to-moderate values of τ^2. However, benchmark (*i*) often becomes unfeasible: since the number of constraints exceeds three, the SDR approach is not tight and it is difficult to find a rank-one solution that simultaneously satisfies all design constraints, which occurs in about 40% of the trials. Relaxing the CM constraints as in Sec. 3.1, the proposed method provides a solution satisfying all design constraints under total power constraints, but projecting it onto $\mathbb{V}^{M_{\text{T}}}$ to impose CM constraints, as benchmark (*iii*) does, frequently violates the SI constraint for moderately stringent η^2; the probability of this event is about 20% with $\eta^2 = 25$ dB, rising to 49% at $\eta^2 = 15$ dB, so this benchmark likely provides unfeasible CM analog beamformers. A similar issue arises with benchmark (*iv*): the relaxed solution can be obtained via SDR, but its projection onto $\mathbb{V}^{M_{\text{T}}}$ almost surely violates the SI constraint, making it unfeasible in CM settings.

5. CONCLUSIONS

We have addressed the design of multibeam analog beamformers for monostatic ISAC under SI. For cases in which the analog array is equipped with per-antenna VGAs and the CM constraints are relaxed, we have derived a semi-analytic solution in which only the Lagrange multipliers have to be numerically computed. For analog phased arrays without VGAs, we have proposed a modified design based on projecting the relaxed solution onto the feasible set at each iteration, simultaneously enforcing all design constraints and achieving communication-sensing performance closed to the upper bound.

Although we have adopted a narrowband model, the proposed CM-constrained transmit beamformer design can be readily extended to practical broadband mmWave scenarios, since fully-analog transmit beamformer is frequency-independent.

APPENDICES

A. STRUCTURE OF THE SOLUTION TO (8)

Let $\boldsymbol{A} \succeq \boldsymbol{0}$, $\boldsymbol{B} \succeq \boldsymbol{0}$, $\boldsymbol{C} \succeq \boldsymbol{0}$, and consider the problem

$$\max_{\boldsymbol{x} \in \mathbb{C}^m} \quad \boldsymbol{x}^H \boldsymbol{A} \boldsymbol{x} \tag{21a}$$

$$\text{s.t.} \quad \boldsymbol{x}^H \boldsymbol{B} \boldsymbol{x} \geq b^2,\ \boldsymbol{x}^H \boldsymbol{C} \boldsymbol{x} \leq c^2,\ \|\boldsymbol{x}\|^2 = m. \tag{21b}$$

Let $\mu \geq 0$, $\gamma \geq 0$ and λ be the Lagrange multipliers respectively associated with the three constraints in (21b). Defining $\boldsymbol{H}(\mu, \gamma) \triangleq \boldsymbol{A} + \mu \boldsymbol{B} - \gamma \boldsymbol{C}$, the Lagrangian for (21) reads $\mathcal{L}(\boldsymbol{x}, \mu, \gamma, \lambda) = \boldsymbol{x}^H(-\boldsymbol{H}(\mu, \gamma) + \lambda \boldsymbol{I}_m)\boldsymbol{x} + \mu b^2 - \gamma c^2 - \lambda m$. Equating to zero the gradient of $\mathcal{L}(\boldsymbol{x}, \mu, \gamma, \lambda)$ with respect to $\boldsymbol{x}$, it is seen that the optimal $\boldsymbol{x}$ must be an eigenvector of $\boldsymbol{H}(\mu, \gamma)$ with eigenvalue λ.

Let $\mathcal{F}$ be the feasible set for (21). The dual function $g(\mu, \gamma, \lambda) = \inf_{\boldsymbol{x} \in \mathcal{F}} \mathcal{L}(\boldsymbol{x}, \mu, \gamma, \lambda)$, is bounded below as long as $\boldsymbol{H}(\mu, \gamma) \preceq \lambda \boldsymbol{I}_m$. Then, it is seen that the value of λ maximizing g is the maximum eigenvalue of $\boldsymbol{H}(\mu, \gamma)$, denoted by $\sigma_1(\mu, \gamma)$, and $\tilde{g}(\mu, \gamma) \triangleq \max_\lambda g(\mu, \gamma, \lambda)$ s.t. $\boldsymbol{H}(\mu, \gamma) \preceq \lambda \boldsymbol{I}_m$ equals $\tilde{g}(\mu, \gamma) = \mu b^2 - \gamma c^2 - m\sigma_1(\mu, \gamma)$. This is upper bounded by the objective function [29, Ch. 5], so that $\mu b^2 - \gamma c^2 - m\sigma_1(\mu, \gamma) \leq -\boldsymbol{x}^H \boldsymbol{A} \boldsymbol{x}, \forall \boldsymbol{x} \in \mathcal{F}$, reflecting the duality gap. Suppose one can find $\mu_\star, \gamma_\star$ such that, with $\boldsymbol{x}_\star = \sqrt{m}\mathcal{D}[\boldsymbol{H}(\mu_\star, \gamma_\star)]$, it holds that $\boldsymbol{x}_\star^H \boldsymbol{B} \boldsymbol{x}_\star = b^2$ and $\boldsymbol{x}_\star^H \boldsymbol{C} \boldsymbol{x}_\star = c^2$. Then it follows that $\mu_\star b^2 - \gamma_\star c^2 - m\sigma_1(\mu_\star, \gamma_\star) = -\boldsymbol{x}_\star^H \boldsymbol{A} \boldsymbol{x}_\star$, so the duality gap is zero, and $\boldsymbol{x}_\star$ is optimal.

B. COMPUTATION OF THE JACOBIAN MATRIX

Each entry of the Jacobian matrix has the same generic structure:

$$\frac{\partial}{\partial \alpha_i}\left(\boldsymbol{u}^H \boldsymbol{P} \boldsymbol{u} - p^2\right), \quad i \in \{1, 2\} \tag{22}$$

where $\boldsymbol{u}$ is the principal eigenvector of $\boldsymbol{M} = (1 - \boldsymbol{\alpha}^T \boldsymbol{1})\boldsymbol{A} + \alpha_1 \boldsymbol{B} - \alpha_2 \boldsymbol{C}$, $\boldsymbol{P} \succeq \boldsymbol{0}$, and $p \in \mathbb{R}$. The partial derivative in (22) amounts to $\dot{\boldsymbol{u}}_i^H \boldsymbol{P} \boldsymbol{u} + \boldsymbol{u}^H \boldsymbol{P} \dot{\boldsymbol{u}}_i$, where $\dot{\boldsymbol{u}}_i \triangleq \partial \boldsymbol{u}/\partial \alpha_i$. From [30] one has $\dot{\boldsymbol{u}}_i = \boldsymbol{V} \boldsymbol{T}_i \boldsymbol{e}_1$, where $\boldsymbol{V}$ is the eigenmatrix of $\boldsymbol{M}$, $\boldsymbol{e}_1$ is the first column of $\boldsymbol{I}_{M_{\text{T}}}$, and $\boldsymbol{T}_i$ is a skew-Hermitian matrix with entries $[\boldsymbol{T}_i]_{k\ell} = t_{k\ell}(i)$, $1 \leq k, \ell \leq M_{\text{T}}$. For $k \neq \ell$, one has $t_{k\ell}(i) = \boldsymbol{v}_k^H \dot{\boldsymbol{M}}_i \boldsymbol{v}_\ell / (\lambda_\ell - \lambda_k)$, where $\dot{\boldsymbol{M}}_i \triangleq \partial \boldsymbol{M}/\partial \alpha_i$, $\boldsymbol{v}_k$ is the k-th eigenvector of $\boldsymbol{M}$, and λ_k is its associated eigenvalue. For $k = \ell$, the coefficients $t_{kk}(i)$ are purely imaginary, but their expression is unknown. As it turns out, (22) does not depend on $\{t_{kk}(i)\}$, as shown next.

Let us write $\boldsymbol{T}_i = \boldsymbol{Z}_i + \imath \boldsymbol{D}_i$, where $\boldsymbol{D}_i$ is a real diagonal matrix with entries $\text{Im}\{t_{kk}(i)\}$, $1 \leq k \leq M_{\text{T}}$, and $\boldsymbol{Z}_i$ is obtained from $\boldsymbol{T}_i$ after setting its diagonal entries to zero. Then, note that $\dot{\boldsymbol{u}}_i = \boldsymbol{V} \boldsymbol{T}_i \boldsymbol{e}_1 = \boldsymbol{V} \boldsymbol{Z}_i \boldsymbol{e}_1 + \imath \boldsymbol{V} \boldsymbol{D}_i \boldsymbol{e}_1 = \boldsymbol{V} \boldsymbol{Z}_i \boldsymbol{e}_1 + \imath \text{Im}\{t_{11}(i)\} \boldsymbol{V} \boldsymbol{e}_1$. Substituting this in (22), and recalling that $\boldsymbol{u} = \boldsymbol{V} \boldsymbol{e}_1$, it is found that

$$\frac{\partial}{\partial \alpha_i}\left(\boldsymbol{u}^H \boldsymbol{P} \boldsymbol{u} - p^2\right) = \boldsymbol{e}_1^H \boldsymbol{Z}_i^H \boldsymbol{V}^H \boldsymbol{P} \boldsymbol{u} + \boldsymbol{u}^H \boldsymbol{P} \boldsymbol{V} \boldsymbol{Z}_i \boldsymbol{e}_1, \tag{23}$$

which does not depend on $\boldsymbol{D}_i$.

6. REFERENCES

[1] N. González-Prelcic, M. F. Keskin, O. Kaltiokallio, M. Valkama, D. Dardari, X. Shen, Y. Shen, M. Bayraktar, and H. Wymeersch, "The integrated sensing and communication revolution for 6G," *Proc. IEEE*, vol. 112, pp. 676–723, 2024.

[2] A. Ghosh, T. N. Wild, J. Du, J. Tan, A. Grudnitsky, D. Chizhik, S. Mandelli, Y. Xing, F. Schaich, and H. Viswanathan, "A unified future: Integrated sensing and communication (ISAC) in 6G," *IEEE J. Sel. Topics Electr., Antennas Propag.*, 2025.

[3] D. K. Pin Tan, J. He, Y. Li, A. Bayesteh, Y. Chen, P. Zhu, and W. Tong, "Integrated sensing and communication in 6G," in *IEEE Int. Online Symp. Joint Commun. & Sens.*, 2021, pp. 1–6.

[4] W. Zhou, R. Zhang, G. Chen, and W. Wu, "Integrated sensing and communication waveform design: A survey," *IEEE Open J. Commun. Soc.*, vol. 3, pp. 1930–1949, 2022.

[5] C. B. Barneto, M. Turunen, S. D. Liyanaarachchi, L. Anttila, A. Brihuega, T. Riihonen, and M. Valkama, "High-accuracy radio sensing in 5G new radio networks: Prospects and self-interference challenge," in *Asilomar Conf. Signals, Syst., Comput.*, 2019, pp. 1159–1163.

[6] K. V. Mishra, M.R. Bhavani Shankar, V. Koivunen, B. Ottersten, and S. A. Vorobyov, "Toward millimeter-wave joint radar communications: A signal processing perspective," *IEEE Signal Process. Mag.*, vol. 36, no. 5, pp. 100–114, 2019.

[7] S. Kutty and D. Sen, "Beamforming for millimeter wave communications: An inclusive survey," *IEEE Commun. Surveys Tut.*, vol. 18, no. 2, pp. 949–973, 2016.

[8] J. A. Zhang, F. Liu, C. Masouros, R. W. Heath, Z. Feng, L. Zheng, and A. Petropulu, "An overview of signal processing techniques for joint communication and radar sensing," *IEEE J. Sel. Topics Signal Process.*, vol. 15, pp. 1295–1315, 2021.

[9] W. Hong, Z. H. Jiang, C. Yu, J. Zhou, P. Chen, Z. Yu, H. Zhang, B. Yang, X. Pang, M. Jiang, Y. Cheng, M. K. T. Al-Nuaimi, Y. Zhang, J. Chen, and S. He, "Multibeam antenna technologies for 5G wireless communications," *IEEE Trans. Antennas Propag.*, vol. 65, no. 12, pp. 6231–6249, 2017.

[10] J. A. Zhang, X. Huang, Y. J. Guo, J. Yuan, and R. W. Heath, "Multibeam for joint communication and radar sensing using steerable analog antenna arrays," *IEEE Trans. Veh. Technol.*, vol. 68, no. 1, pp. 671–685, 2019.

[11] C. B. Barneto, T. Riihonen, S. D. Liyanaarachchi, M. Heino, N. González-Prelcic, and M. Valkama, "Beamformer design and optimization for joint communication and full-duplex sensing at mm-Waves," *IEEE Trans. Commun.*, vol. 70, no. 12, pp. 8298–8312, 2022.

[12] A. Liu, T. Riihonen, and W. Sheng, "Full-duplex analog beamforming design for mm-Wave integrated sensing and communication," in *IEEE Radar Conf.*, 2023, pp. 1–6.

[13] R. Hersyandika, A. Sakhnini, Y. Miao, Q. Wang, and S. Pollin, "Guard beams: Coverage enhancement of UE-centered ISAC via analog multi-beamforming," *IEEE Access*, vol. 12, pp. 163507–163523, 2024.

[14] Q. Wan, S. Ma, J. Fang, and Y. Wu, "Robust closed-form multibeam beamforming design for mmWave dual-function radar-communication systems," *IEEE Internet Things J.*, vol. 11, no. 22, pp. 36801–36816, 2024.

[15] M. Bayraktar, N. González-Prelcic, and H. Chen, "Hybrid precoding and combining for mmWave full-duplex joint radar and communication systems under self-interference," in *IEEE Int. Conf. Commun. (ICC)*, 2024, pp. 915–920.

[16] Y. Luo, J. A. Zhang, X. Huang, W. Ni, and J. Pan, "Optimization and quantization of multibeam beamforming vector for joint communication and radio sensing," *IEEE Trans. Commun.*, vol. 67, no. 9, pp. 6468–6482, 2019.

[17] Y. Luo, J. A. Zhang, X. Huang, W. Ni, and J. Pan, "Multibeam optimization for joint communication and radio sensing using analog antenna arrays," *IEEE Trans. Veh. Technol.*, vol. 69, no. 10, pp. 11000–11013, 2020.

[18] F. Liu, L. Zhou, C. Masouros, A. Li, W. Luo, and A. Petropulu, "Toward dual-functional radar-communication systems: Optimal waveform design," *IEEE Trans. Signal Process.*, vol. 66, no. 16, pp. 4264–4279, 2018.

[19] F. Liu, C. Masouros, A. Li, H. Sun, and L. Hanzo, "MU-MIMO communications with MIMO radar: From co-existence to joint transmission," *IEEE Trans. Wireless Commun.*, vol. 17, no. 4, pp. 2755–2770, 2018.

[20] Z. Liu, S. Aditya, H. Li, and B. Clerckx, "Joint transmit and receive beamforming design in full-duplex integrated sensing and communications," *IEEE J. Sel. Areas Commun.*, vol. 41, no. 9, pp. 2907–2919, 2023.

[21] H. Liu, Y. Zhuo, S. Jin, and Z. Wang, "Robust beamforming for multi-beam ISAC systems," *IEEE Wireless Commun. Lett.*, vol. 14, no. 7, pp. 2049–2053, 2025.

[22] Md A. Islam, G. C. Alexandropoulos, and B. Smida, "Integrated sensing and communication with millimeter wave full duplex hybrid beamforming," in *IEEE Int. Conf. Commun. (ICC)*, 2022, pp. 4673–4678.

[23] S. Ghosh and D. Sen, "An inclusive survey on array antenna design for millimeter-wave communications," *IEEE Access*, vol. 7, pp. 83137–83161, 2019.

[24] G. Chai, Z. Yu, M. Nabeel, X. Wu, and G. Caire, "Constant modulus constrained codebook synthesis for self-interference suppression in integrated sensing and communication at mmWave," in *2024 Joint European Conf. Netw. and Commun. & 6G Summit (EuCNC/6G Summit)*, 2024, pp. 387–391.

[25] Z.-Q. Luo, W.-K. Ma, A. M.-C. So, Y. Ye, and S. Zhang, "Semidefinite relaxation of quadratic optimization problems," *IEEE Signal Process. Mag.*, vol. 27, no. 3, pp. 20–34, 2010.

[26] Y. Huang and D. P. Palomar, "Rank-constrained separable semidefinite programming with applications to beamforming," *IEEE Trans. Signal Process.*, vol. 58, pp. 664–678, 2010.

[27] S. M. Kay, *Fundamentals of statistical signal processing: estimation theory*, Prentice-Hall, Inc., 1993.

[28] R. López-Valcarce and M. Martínez-Cotelo, "Full-duplex mmWave MIMO with finite-resolution phase shifters," *IEEE Trans. Wireless Commun.*, vol. 21, pp. 8979–8994, 2022.

[29] S. Boyd and L. Vandenberghe, *Convex Optimization*, Cambridge University Press, 2004.

[30] N. P. Van der Aa, H. G. Ter Morsche, and R. M. M. Mattheij, "Computation of eigenvalue and eigenvector derivatives for a general complex-valued eigensystem," *Elec. J. Linear Algebra*, vol. 16, pp. 300–314, 2007.